nature medicine

Recurrent *MET* fusion genes represent a drug target in pediatric glioblastoma

Sebastian Bender[1–3,40], Jan Gronych[3,4,40], Hans-Jörg Warnatz[5,40], Barbara Hutter[6,40], Susanne Gröbner[1,3], Marina Ryzhova[7], Elke Pfaff[1–3], Volker Hovestadt[3,4], Florian Weinberg[8,9], Sebastian Halbach[8], Marcel Kool[1,3], Paul A Northcott[1,3], Dominik Sturm[1–3], Lynn Bjerke[10], Thomas Zichner[11], Adrian M Stütz[11], Kathrin Schramm[3,4], Bingding Huang[12], Ivo Buchhalter[6,12], Michael Heinold[6], Thomas Risch[5], Barbara C Worst[1–3], Cornelis M van Tilburg[2,3,13], Ursula D Weber[3,4], Marc Zapatka[3,4], Benjamin Raeder[11], David Milford[14], Sabine Heiland[14], Christof von Kalle[15,16], Christopher Previti[16], Chris Lawerenz[12], Andreas E Kulozik[2], Andreas Unterberg[17], Olaf Witt[2,18], Andreas von Deimling[3,19,20], David Capper[3,19,20], Nathalène Truffaux[21,22], Jacques Grill[21,22], Nada Jabado[23,24], Astrid M Sehested[25], David Sumerauer[26], Dorra Hmida-Ben Brahim[27], Saoussen Trabelsi[27], Ho-Keung Ng[28], David Zagzag[29,30], Jeffrey C Allen[31], Matthias A Karajannis[31], Nicholas G Gottardo[32–34], Chris Jones[10], Jan O Korbel[11], Sabine Schmidt[16], Stephan Wolf[16], Guido Reifenberger[35], Jörg Felsberg[35], Benedikt Brors[3,6,13], Christel Herold-Mende[17], Hans Lehrach[5], Tilman Brummer[8,9,36,37], Andrey Korshunov[3,19,20], Roland Eils[12,38,39], Marie-Laure Yaspo[5], Stefan M Pfister[1–3,41], Peter Lichter[3,4,41] & David T W Jones[1,3,41], for the International Cancer Genome Consortium PedBrain Tumor Project

Pediatric glioblastoma is one of the most common and most deadly brain tumors in childhood. Using an integrative genetic analysis of 53 pediatric glioblastomas and five *in vitro* model systems, we identified previously unidentified gene fusions involving the *MET* oncogene in ~10% of cases. These *MET* fusions activated mitogen-activated protein kinase (MAPK) signaling and, in cooperation with lesions compromising cell cycle regulation, induced aggressive glial tumors *in vivo*. MET inhibitors suppressed MET tumor growth in xenograft models. Finally, we treated a pediatric patient bearing a MET-fusion-expressing glioblastoma with the targeted inhibitor crizotinib. This therapy led to substantial tumor shrinkage and associated relief of symptoms, but new treatment-resistant lesions appeared, indicating that combination therapies are likely necessary to achieve a durable clinical response.

Pediatric glioblastoma is a deadly childhood tumor that is characterized by a complex genomic landscape and profound heterogeneity[1–3]. Certain canonical pathways, however, such as the MAPK or phosphatidylinositol 3-kinase (PI3K) pathways, are frequently deregulated. The identification of recurrent mutations of histone H3-encoding genes (most commonly *H3F3A*) and chromatin modifiers such as *ATRX* also suggests that epigenetic deregulation has a prominent role in pediatric glioblastoma[4,5]. Standard treatment is based on nonselective radio- and chemotherapy, with marginal clinical benefit. No molecularly targeted therapy is currently used. Patient outcomes remain dismal, and new targets for individualized or molecularly stratified therapies are desperately needed.

We performed whole-genome sequencing of tumor and blood DNA from 53 samples (**Supplementary Table 1**), as well as from five pediatric glioblastoma cell lines covering the whole spectrum of recurrent H3.3 mutations, in the context of the International Cancer Genome Consortium (ICGC) PedBrain Tumor project (**Fig. 1** and **Supplementary Tables 2** and **3**). Genome-wide DNA methylation analysis on our cohort revealed that, in addition to the previously described epigenetic subgroups[6], five of the tumors molecularly resembled pleomorphic xanthoastrocytoma (PXA)[7], a less aggressive brain tumor with heterogeneous appearance[3] (**Supplementary Fig. 1**). The full tumor cohort is described in **Supplementary Tables 1** and **2**. Two of five PXA-like tumors carried lesions that are typical of PXAs (*BRAF* V600E and deletion of *CDKN2A* and *CDKN2B*)[8,9]. Moreover, one potential PXA (ICGC_GBM34) in an infant was found to harbor a gene fusion between Ets variant 6 (*ETV6*) and the neurotrophin receptor type 2 (*NTRK2*) gene. This fusion, and others involving *NTRK*-family genes, have been identified in 40% of infant glioblastomas[10] and some lower-grade gliomas[11,12]. Analogous to the highly oncogenic FGFR1-TACC1 and FGFR3-TACC3 fusions in glioblastoma[13], we found a previously unknown fusion of fibroblast growth factor receptor 2 (*FGFR2*) with CAP-GLY-domain-containing linker protein 2 (*CLIP2*) in a molecular PXA primary-relapse pair (ICGC_GBM19&50) (**Supplementary Table 4**). Three pediatric glioblastomas whose DNA methylation profiles clustered together with normal brain samples (suggesting high

A full list of affiliations appears at the end of the paper.

Received 19 October 2015; accepted 15 September 2016; published online 17 October 2016; doi:10.1038/nm.4204

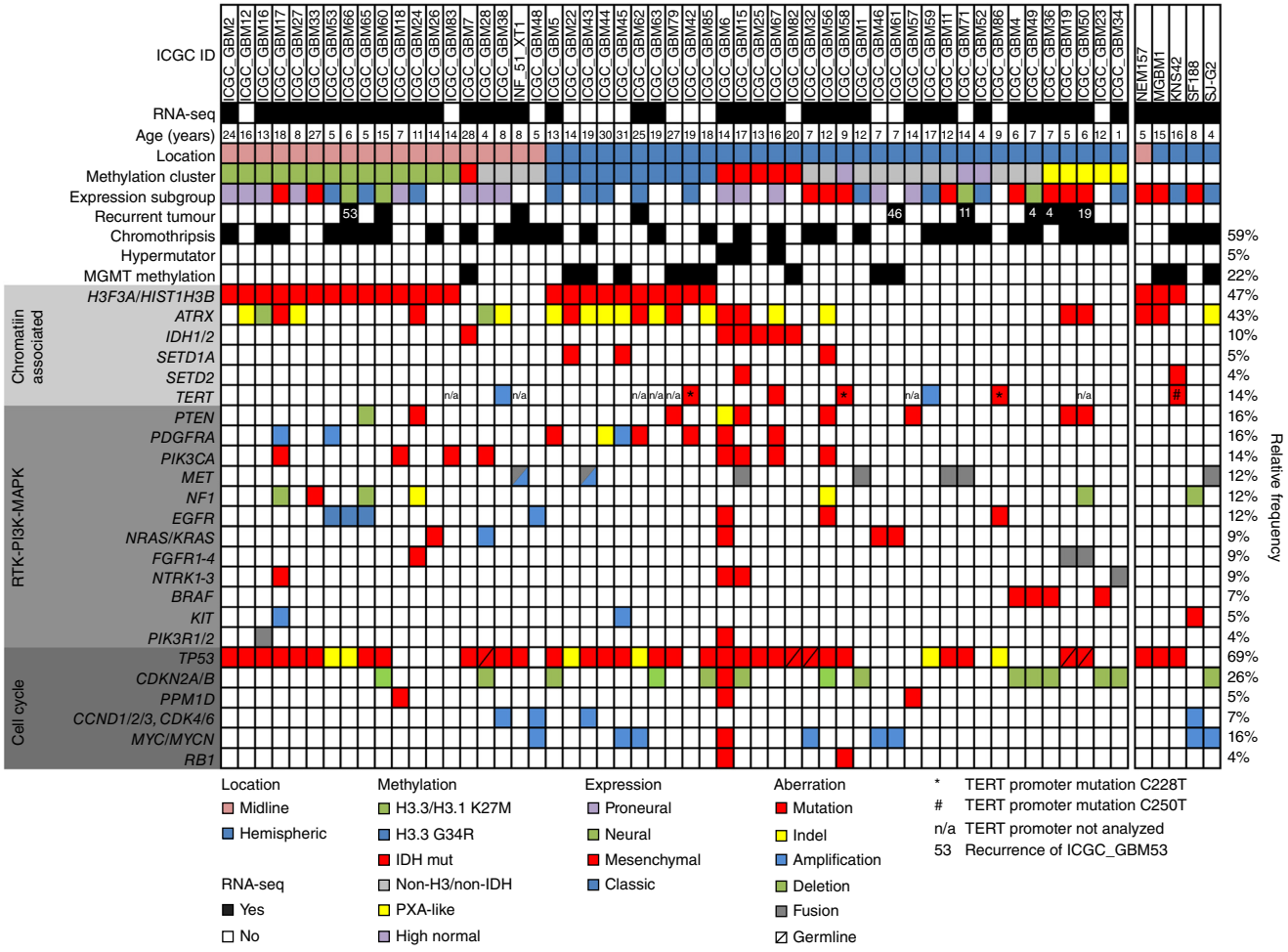

Figure 1 The genomic landscape of pediatric glioblastomas. Genetic alterations (mutations, small insertions/deletions (InDels), focal copy number alterations and fusions) identified by whole-genome (n = 52) or whole-exome/low-coverage whole-genome (INF_51_XT1) and RNA-sequencing (n = 42) in 19 midline and 29 hemispheric pediatric glioblastomas, five PXA-like tumors and five pediatric glioblastoma cell lines. Frequencies of genetic alterations in 58 analyzed samples are indicated at the end of each row. Numbers given in the recurrent tumor row indicate the ICGC identification numbers of the respective primary tumors.

normal cell content) showed notably lower-than-expected mutant allele frequencies (**Supplementary Fig. 2**).

A full overview of genetic alterations is provided in **Figure 1** and **Supplementary Table 3**. The most commonly altered pathway was cell cycle regulation, with mutations in *TP53* or *PPM1D*, or homozygous deletion of *CDKN2A* and *CDKN2B*, being identified in 83% of all samples. We also detected numerous genetic lesions that are likely to result in aberrantly activated receptor tyrosine kinase (RTK)-PI3K-MAPK signaling, including activating mutations of RTKs (for example, *EGFR*) or downstream proteins (for example, *NRAS*, *KRAS*, *BRAF* and *PIK3CA*) and high-level gene amplifications of *EGFR*, *PDGFR/KIT* or *MET* (**Fig. 1**). ICGC_GBM17 harbored a previously unknown splice site mutation in intron 12 of *NTRK3*, likely resulting in an amino-terminally truncated protein that maintained the catalytically active NTRK3 kinase domain (**Supplementary Fig. 3**). Other common features included a high frequency of marked structural rearrangements (chromothripsis)[14], hypermutated tumors (before any adjuvant therapy, and often associated with germline mismatch repair deficiency[15]) and alterations in telomere maintenance. Analysis of five primary-recurrent tumor pairs revealed that known somatic driver events were typically shared between primary and recurrent lesions, with the exception of ICGC_GBM11 and ICGC_GBM71 (which were clinically reported as two anatomically distinct lesions; **Supplementary Fig. 4**). Notably, different *BCOR* gene mutations were detected in the primary tumor (ICGC_GBM4, *BCOR* F206fs) and both recurrent tumors (ICGC_GBM36, *BCOR* wild type and ICGC_GBM49, *BCOR* V1112fs) of one patient (**Supplementary Fig. 4**).

RNA sequencing revealed fusion transcripts that were the results of structural rearrangements in most samples (27 of 42, 64%; **Supplementary Table 4**). These often involved known cancer-associated genes, such as *FGFR2*, *NTRK2* and *PIK3R2*. The most frequently affected gene was *MET*, which encodes an oncogenic tyrosine kinase. We detected two previously unknown fusions of MET that retained only the carboxy-terminal kinase domain. In ICGC_GBM1, the MET kinase domain was fused to TRK-fused gene (TFG), which was previously described to form chimeric proteins with other RTKs, such as NTRK1 in papillary thyroid carcinoma or ALK in anaplastic large-cell lymphoma[16,17]. The pediatric glioblastoma cell line SJ-G2 (ICGC_GBM41) harbored a *CLIP2-MET* fusion (**Fig. 2a**). For the first time in the pediatric setting, to the best of our knowledge, we also identified two primary pediatric glioblastomas with a *PTPRZ1-MET* fusion[18]. In this variant, expression of full-length MET was

driven from the highly active *PTPRZ1* promoter, leading to MET overexpression (**Supplementary Fig. 5a**,**b**). In two additional tumors without RNA-seq data, copy number analysis suggested the presence of a *PTPRZ1-MET* fusion, which we subsequently confirmed by PCR (ICGC_GBM43 and ICGC_GBM71). Dual-color fluorescence *in situ* hybridization detected the *PTPRZ1-MET* fusion in tumor sections of ICGC_GBM11, ICGC_GBM15 and ICGC_GBM71 (**Supplementary Fig. 5c**). ICGC_GBM43 (H3.3 G34R) was the only histone H3.3-mutant tumor harboring a *MET* fusion and amplification. Notably, all pediatric glioblastomas bearing a *MET* fusion were found to have impaired cell cycle regulation as a result of *TP53* mutation or homozygous deletion of the *CDKN2A* and *CDKN2B* locus (**Fig. 1**). DNA methylation and gene expression did not show MET-fusion-bearing pediatric glioblastomas as clustering separately. None of the tumors expressed the short variant of *MET* lacking exons 7 and 8, which was recently described in 6% of high-grade gliomas[19].

Overexpression of hemagglutinin (HA)-tagged TFG-MET or PTPRZ1-MET in HEK293T cells resulted in the phosphorylation of tyrosines Y1234 and Y1235 in the activation loop of the kinase domain (**Fig. 2b**). Moreover, this overexpression induced strong activation of MAPK signaling, as indicated by substantially elevated pERK levels (**Fig. 2b**), and resulted in cell rounding and detachment (**Supplementary Fig. 6a**)[20]. Notably, the amino-terminally truncated fusions showed much higher downstream activity than the full-length, *PTPRZ1*-driven variant (**Fig. 2b**).

To further characterize induced transcriptional changes in a model that better mimics the presumed origins of pediatric glioblastoma, we generated expression profiles of TFG-MET-overexpressing normal human astrocytes. Transduced cells displayed a phenotypic change that was indicative of transformation (**Supplementary Fig. 6a**,**b**), as well as altered expression of multiple factors involved in MAPK signaling (for example, MAP2K3, MAP2K6 and DUSP14) and downstream transcription factors (for example, FOS and JUN) (**Supplementary Fig. 6c** and **Supplementary Table 5**).

TFG-MET-overexpressing cells were subsequently treated with the MET inhibitors foretinib, SGX523 or crizotinib, which abrogated MET-fusion-induced MAPK activation (**Fig. 2b**,**c**). In CLIP2-MET-expressing SJ-G2 cells, foretinib reduced cell viability in a concentration-dependent manner, resulting in a half-maximum inhibition concentration (IC_{50}) of 0.8 µM. In three pediatric glioblastoma cell lines without MET fusion, the IC_{50} was substantially higher (2–13.5 µM; **Supplementary Fig. 6d**). Although the methylated *MGMT* promoter may suggest sensitivity to alkylating therapy, temozolomide (the current standard chemotherapeutic for pediatric glioblastoma) did not affect the viability of SJ-G2 cells, even at concentrations of >300 µM (**Supplementary Fig. 6e**). Anchorage-independent growth of these cells was also completely abolished in the presence of 0.5 µM foretinib (**Supplementary Fig. 6f**).

To test the oncogenicity of MET fusions *in vivo*, we used the RCAS/Tv-a somatic gene transfer system to introduce the TFG-MET fusion (PTPRZ1-MET fusions exceed the RCAS insert size limit of ~2.5 kb) into nestin-positive cells of wild-type (Ntv-a), Cdkn2a-deficient (Ntv-a; *Cdkn2a*$^{-/-}$; *Pten*$^{fl/fl}$) or p53-null (Ntv-a; *Trp53*$^{-/-}$) neonatal mice. Although no tumors could be found in wild-type mice ($n = 7$) by 12 weeks after injection, *Cdkn2a*$^{-/-}$ ($n = 7$) and *Trp53*$^{-/-}$ mice ($n = 5$) rapidly developed severe neurological symptoms and extensive contrast-enhancing lesions (**Fig. 3a**,**b**). Neuropathological evaluation revealed histology that was characteristic of that of high-grade glioma, and immunohistochemistry detected expression of the HA-tagged fusion protein, as well as

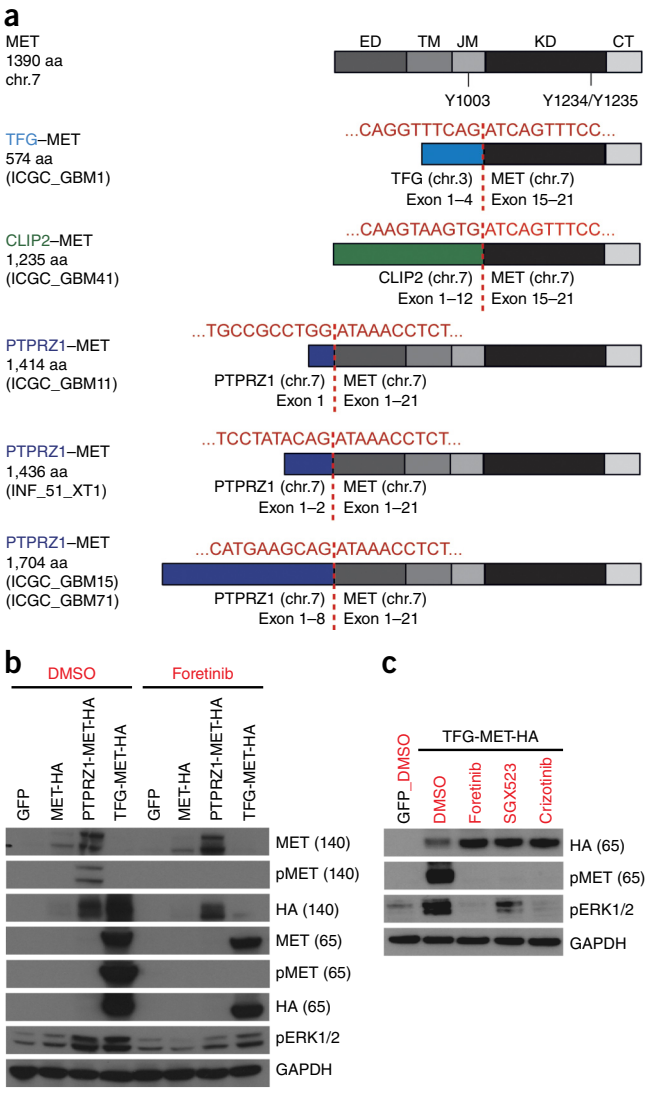

Figure 2 Oncogenic MET fusions. (**a**) Schematics of wild-type MET and fusion proteins identified in pediatric glioblastomas. The MET polypeptide precursor is composed of the extracellular domain (ED), the transmembrane domain (TM), the juxtamembrane domain (JM), the kinase domain (KD) and the carboxy-terminal domain (CT). Tyrosine 1003 (Y1003) negatively regulates MET by recruiting ubiquitin ligases. Tyrosines 1234 and 1235 (Y1234/Y1235) are crucial for MET activation. TFG-MET and CLIP2-MET maintain only the kinase domain, whereas PTPRZ1-MET fusion proteins contain full-length MET. (**b**) HA-tagged MET fusions (TFG-MET or PTPRZ1-MET) or wild-type MET were expressed in HEK293 cells. We measured the abundance of indicated proteins by immunoblot. Cells were treated with 0.5 µM foretinib for 24 h where indicated. Proteins at 140 kDA represent endogenous (wild-type) MET or overexpressed PTPRZ1-MET-HA; overexpressed TFG-MET-HA protein had a molecular weight of 65 kDa. (**c**) MET-fusion-overexpressing HEK293T cells were treated where indicated with the MET inhibitors foretinib (0.5 µM), SGX523 (1 µM) or crizotinib (1 µM) for 24 h.

phosphorylated MET and Erk (**Fig. 3c**). A contribution of off-target viral mutagenesis to tumorigenesis in this system can be excluded on the basis of previously published data[21] and our own unpublished observations (J. Gronych).

As a result of the rapid growth of RCAS-driven tumors and the lack of reliable techniques for oral drug delivery in infant mice (younger than postnatal day 10), we used luciferase-labeled RCAS-TFG-MET-driven

mouse tumor cells that were allografted into the striatum of 6–8-week-old immunocompromised mice to assess pharmacological MET inhibition *in vivo*. We split the mice into two groups with similar distributions of luminescence intensity 1 week after transplantation and subsequently subjected them to a 60 mg per kg foretinib versus vehicle 1 d on/1 d off treatment regimen. Foretinib treatment significantly

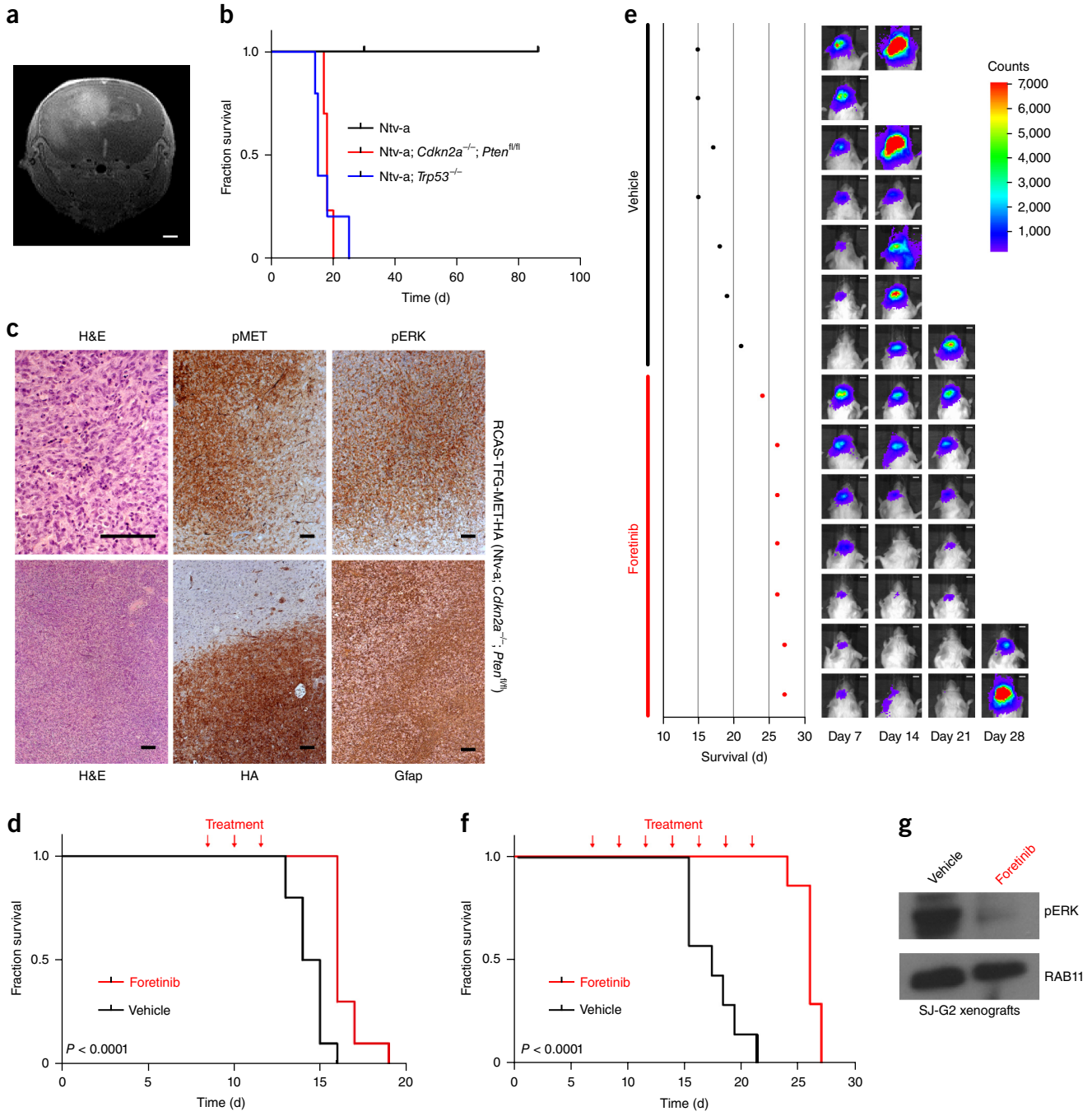

Figure 3 MET fusion animal model and preclinical testing of a MET inhibitor. (**a**) We injected 10^5 DF-1 cells producing RCAS-TFG-MET-HA viral particles into the cerebral hemisphere of neonatal Ntv-a; *Cdkn2*$^{-/-}$; *Pten*$^{fl/fl}$ animals. MRI imaging (T1 RARE) of an Ntv-a; *Cdkn2a*$^{-/-}$; *Pten*$^{fl/fl}$ animal 2 weeks after inoculation with RCAS-TFG-MET-HA virus is shown. Scale bar represents 1 mm. (**b**) Kaplan–Meier survival analysis of wild-type (Ntv-a), Cdkn2a-null (Ntva; *Cdkn2a*$^{-/-}$; *Pten*$^{fl/fl}$) and p53-null (Ntv-a; *Trp53*$^{-/-}$) mice inoculated with RCAS-TFG-MET ($P = 0.0001$). (**c**) Histologic analysis of a tumor induced by overexpression of TFG-MET in Ntv-a; *Cdkn2a*$^{-/-}$; *Pten*$^{fl/fl}$ animals. Scale bars represent 100 µm. (**d**) Luciferase-labeled murine RCAS-TFG-MET tumor cells were implanted into the striatum of adult C.B-17 SCID mice and treated with 60 mg/kg foretinib ($n = 10$) or vehicle ($n = 10$) every other day starting 1 week after surgery. Kaplan–Meier analysis of survival revealed a significant survival benefit for animals treated with foretinib ($P < 0.0001$). (**e**) C.B-17 SCID animals were transplanted with luciferase-labeled CLIP2-MET-expressing SJ-G2 cells and subjected to intravital bioluminescence imaging once a week. Mice were treated with 60 mg/kg foretinib ($n = 7$) or vehicle ($n = 7$) every other day starting 7 d after surgery. Intravital bioluminescence imaging was performed once a week. Scale bars represent 5 mm. (**f**) Kaplan–Meier analysis of the mice described in **e** ($P < 0.0001$). (**g**) Immunoblot analysis of protein extracts from SJ-G2 xenografts of a foretinib-treated and an untreated (vehicle) mouse from an independent experiment with antibodies detecting phosphorylated ERK (T202/Y204). RAB11 is shown as a loading control.

decelerated MET-fusion-driven tumor growth ($P < 0.0001$; **Supplementary Fig. 6g**), leading to prolonged overall survival (**Fig. 3d**).

To confirm our results, we established a xenograft model using luciferase-labeled SJ-G2 cells that endogenously harbor the *CLIP2-MET* fusion, which we transplanted intracranially into C.B-17 SCID immunocompromised mice. Tumor growth was monitored once a week by intravital bioluminescence imaging (**Fig. 3e**). Although all of the vehicle-treated animals showed a clear increase in luminescence signal, the signal in foretinib-treated animals stagnated or even decreased under treatment. All foretinib-treated animals were still alive at the end of the 2-week treatment, whereas six of seven of the untreated animals had died (median survival: vehicle, 17 d; foretinib, 26 d; $P = 0.0001$; **Fig. 3f**). Western blot analysis showed reduced ERK phosphorylation in tumor tissue of the foretinib-treated animals, indicating that target inhibition was successful and downstream signaling was reduced (**Fig. 3g**).

Finally, we were able to translate these findings into clinical application in the pilot phase of the INFORM personalized oncology program[22] (German Clinical Trials Register ID: DRKS00007623). Whole-exome, low-coverage whole-genome (for copy number annotation) and RNA sequencing were performed on a recurrent lesion from an 8-year-old male patient treated 3 years previously for a group 3 medulloblastoma (INF_51_XT1). This revealed the presence of a *PTPRZ1-MET* fusion in the recurrent tumor, and subsequent molecular and histological review indicated that this lesion was in fact a cerebellar glioblastoma (that is, most likely a radiation-induced secondary glioblastoma) (**Fig. 4a**). On this basis, the patient received treatment with crizotinib (a Food and Drug Administration–approved kinase inhibitor with activity against MET), which has been shown to induce tumor regression of a *MET*-amplified glioblastoma[23]. Magnetic resonance imaging (MRI) evaluation 2 months after treatment initiation revealed a partial response of the primary lesion with concomitant relief of symptoms. However, several new treatment-resistant lesions were also observed. Rapid progression of those lesions ultimately resulted in the death of the patient (**Fig. 4b**). No autopsy material was available for studying the resistance mechanism.

Oncogenic activation of MET signaling is found in numerous human malignancies, including cancer of the hematopoietic system, carcinomas, sarcomas and glioblastomas[24,25]. In pediatric glioblastomas, *MET* gene amplification has been described in about 3–7% of tumors[10,26], whereas we found that *MET* fusions were present in up to 10% of cases. Notably, the structural alterations in ICGC_GBM11 and ICGC_GBM71, representing two lesions from one patient, suggest that distinct *PTPRZ1-MET* fusions arose separately in each tumor. High clonality of the *PTPRZ1-MET* fusion, as indicated by our fluorescence *in situ* hybridization data, further underlines the likely tumor-initiating character of this fusion, which seems to rely on extremely high expression of full-length MET driven by the *PTPRZ1* promoter. The amino-terminally truncated versions, however, represent cytosolic, constitutively active forms of MET, which escape normal downregulation[27]. The latter are analogous to the oncogenic *TPR-MET* fusion that was originally identified in mutagen-treated osteosarcoma cells[28]. A recent screen of data of the Cancer Genome Atlas interrogating multiple tumor types (http://54.84.12.177/PanCanFusV2/)[29] revealed a small number of *MET* fusions, including one *TFG-MET* fusion, in breast, lung and thyroid cancer, suggesting that *MET* rearrangements may have a broader role across tumor entities.

Our data suggest that MET-fusion-induced tumorigenesis is dependent on additional genetic lesions affecting cell cycle regulation. All seven pediatric glioblastomas bearing a MET fusion harbored mutations of *TP53* or deletions of *CDKN2A* and *CDKN2B*. Accordingly, overexpression of TFG-MET in neural progenitor cells induced aggressive glial brain tumors in Cdkn2a- or Trp53-deficient mice, but not in wild-type animals.

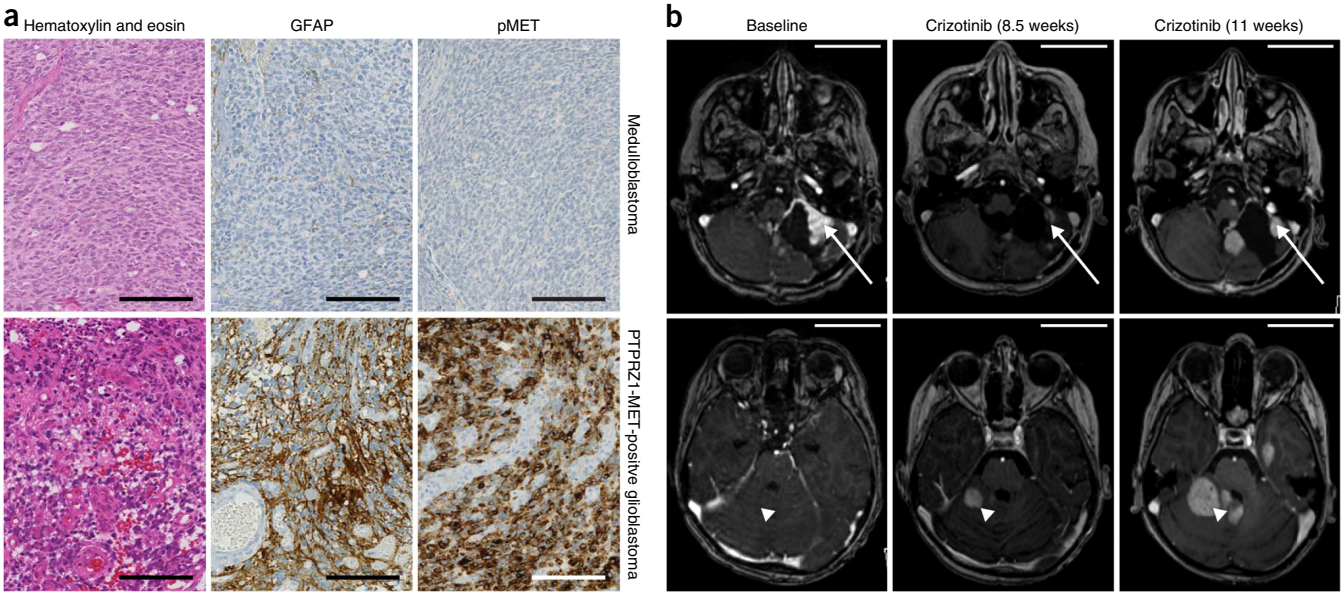

Figure 4 Translation of MET inhibitor treatment into a clinical setting. (**a**) Immunohistochemical staining for hematoxylin and eosin, GFAP and phosphorylated MET (pMET) (Y1234/Y1235) of the primary medulloblastoma (top) and the PTPRZ1-MET-expressing pediatric glioblastoma (bottom) in patient INF_51_XT1. Scale bars represent 100 µm. (**b**) All images represent axial T1-weighted MRI scans with contrast enhancement of patient INF_51_XT1 at baseline and at indicated time points after initiation of treatment. Crizotinib was administered orally at 2 × 250 mg/d (equivalent to 2 × 280 mg/m^2, published recommended phase II dose[33]) for 11 weeks, with a pause from days 13 to 16. Marked tumor shrinkage corresponding to a partial response at the site of the main lesion was observed (arrows). New lesions also developed during the course of treatment (arrowheads). Scale bars represent 5 cm.

On the basis of our preclinical allograft and xenograft data, pharmacological MET inhibition was immediately translated into clinical application by treating a child with a *PTPRZ1-MET* fusion-driven pediatric glioblastoma with a MET inhibitor, leading to a relief of symptoms over a period of 2 months and substantial volume reduction of the primary tumor. Unfortunately, new lesions that developed rapidly under crizotinib monotherapy ultimately led to a fatal outcome. Given that acquired resistance to MET inhibition is a well-known challenge in the treatment of numerous cancers[30,31], combinatorial inhibition of multiple RTKs, as recently described in diffuse intrinsic pontine gliomas[32], might represent a promising therapeutic option.

In conclusion, our results highlight a new recurrent mechanism of tumorigenesis in pediatric glioblastoma and underline the importance of individualized molecular diagnosis for cancer patients as a basis for optimal personalized therapy. Our data also provide strong rationale for the systematic analysis of MET inhibitors in future pediatric glioblastoma clinical trials.

METHODS

Methods and any associated references are available in the online version of the paper.

Accession codes. Short-read sequencing and methylation data are available at the European Genome-phenome Archive (http://www.ebi.ac.uk/ega/), hosted by the European Bioinformatics Institute under the accession number EGAS00001001139.

Note: Any Supplementary Information and Source Data files are available in the online version of the paper.

ACKNOWLEDGMENTS

For technical support and expertise, we thank A. Wittmann, L. Sieber, C. Xanthopoulos, D. Sohn and N. Mack, the DKFZ Genomics and Proteomics Core Facility, the DKFZ Center for Preclinical Research, R. Kabbe (Division of Theoretical Bioinformatics, DKFZ), M. Bieg and M. Schlesner (Division of Applied Bioinformatics, DKFZ), C. Jäger-Schmidt (Data Management Group, DKFZ), S. Rüffer and T. Giese from the Heidelberg University Hospital, M. Rabenstein from the NCT Heidelberg, S. Thamm, D. Balzereit, S. Dökel, M. Linser, A. Kovacsovics and V. Amstislavskiy from the Max Planck Institute for Molecular Genetics (MPIMG) in Berlin, the tissue bank of the National Center for Tumor Diseases (NCT, Heidelberg), and the Department of Oncogenomics (University of Amsterdam). Ntv-a; *Cdkn2a*$^{-/-}$; *Pten*$^{fl/fl}$ mice were kindly provided by E. Holland (Fred Hutchinson Cancer Research Center). This work was principally supported by the PedBrain Tumor Project contributing to the International Cancer Genome Consortium, funded by German Cancer Aid (109252) and by the German Federal Ministry of Education and Research (BMBF, grants #01KU1201A, MedSys #0315416C, NGFNplus #01GS0883 and e:Med Joint Research Projects SYS-GLIO #031A425A and CancerTelSys #01ZX1302). Additional support came from the German Cancer Research Center–Heidelberg Center for Personalized Oncology (DKFZ-HIPO), the German Cancer Consortium (DKTK, INFORM project), the Max Planck Society (Munich, Germany), the European Union (FP7/2007-2013, grant ESGI #262055), the Helmholtz Alliance Preclinical Comprehensive Cancer Center (PCCC, grant number HA-305), the German Research Foundation (DFG, grant LA2983/2-1), the EDM and the Lemos Foundations, the New York University Langone Human Specimen Resource Center, Laura and Isaac Perlmutter Cancer Center, supported in part by the Cancer Center Support Grant, P30 CA16087 from the National Cancer Institute, US National Institutes of Health, UL 1 TR000038 from the National Center for the Advancement of Translational Science (NCATS), US National Institutes of Health, and grants from the Making Headway Foundation. J. Gronych was supported by a Dr. Mildred Scheel Foundation Scholarship. The authors acknowledge NHS funding to the NIHR Biomedical Research Centre at The Royal Marsden and the ICR as well as the project (Ministry of Health, Czech Republic) for conceptual development of research organization 00064203 (University Hospital Motol, Prague, Czech Republic).

AUTHOR CONTRIBUTIONS

S.B., J. Gronych, H.-J.W., E.P., F.W., S. Halbach, D. Sturm, L.B., A.M. Stütz, K.S., B.R., D.M., S. Heiland, C.v.K., S.S., S.W., J.F., T.B. performed and/or coordinated the experimental work. S.B., J. Gronych, H.-J.W., B. Hutter, S.G., V.H., M.K., P.A.N., T.Z., B. Huang, M.R., I.B., M.H., T.R., M.Z., C.P., C.L., B.C.W. performed data analysis. M.R., A.E.K., A.U., O.W., A.v.D., D.C., N.J., A.M. Sehested, D. Sumerauer, M.A.K., C.J., C.H.-M., A.K., J. Grill, N.T., C.M.v.T., B.C.W., D.H.-B.B., S.T., H.-K.N., D.Z., J.C.A., N.G.G. collected data and provided patient materials. S.B., J. Gronych, H.-J.W., B. Hutter, S.M.P., P.L. and D.T.W.J. prepared the initial manuscript and figures. S.B., J. Gronych, U.D.W., J.O.K., G.R., B.B., H.L., T.B., R.E., M.-L.Y., S.M.P., P.L. and D.T.W.J. provided project leadership.

COMPETING FINANCIAL INTERESTS

The authors declare no competing financial interests.

1. Sturm, D. *et al.* Pediatric and adult glioblastoma: multiform (epi)genomic culprits emerge. *Nat. Rev. Cancer* **14**, 92–107 (2014).
2. Jones, C. & Baker, S.J. Unique genetic and epigenetic mechanisms driving pediatric diffuse high-grade glioma. *Nat. Rev. Cancer* **14**, 651–661 (2014).
3. Louis, D.N. *et al. WHO Classification of Tumors of the Central Nervous System, Revised* 4th edn. (IARC, 2016).
4. Wu, G. *et al.* Somatic histone H3 alterations in pediatric diffuse intrinsic pontine gliomas and non-brainstem glioblastomas. *Nat. Genet.* **44**, 251–253 (2012).
5. Schwartzentruber, J. *et al.* Driver mutations in histone H3.3 and chromatin remodeling genes in pediatric glioblastoma. *Nature* **482**, 226–231 (2012).
6. Sturm, D. *et al.* Hotspot mutations in *H3F3A* and *IDH1* define distinct epigenetic and biological subgroups of glioblastoma. *Cancer Cell* **22**, 425–437 (2012).
7. Korshunov, A. *et al.* Integrated analysis of pediatric glioblastoma reveals a subset of biologically favorable tumors with associated molecular prognostic markers. *Acta Neuropathol.* **129**, 669–678 (2015).
8. Dias-Santagata, D. *et al.* BRAF V600E mutations are common in pleomorphic xanthoastrocytoma: diagnostic and therapeutic implications. *PLoS One* **6**, e17948 (2011).
9. Weber, R.G. *et al.* Frequent loss of chromosome 9, homozygous CDKN2A/p14(ARF)/CDKN2B deletion and low TSC1 mRNA expression in pleomorphic xanthoastrocytomas. *Oncogene* **26**, 1088–1097 (2007).
10. Wu, G. *et al.* The genomic landscape of diffuse intrinsic pontine glioma and pediatric non-brainstem high-grade glioma. *Nat. Genet.* **46**, 444–450 (2014).
11. Jones, D.T. *et al.* Recurrent somatic alterations of FGFR1 and NTRK2 in pilocytic astrocytoma. *Nat. Genet.* **45**, 927–932 (2013).
12. Zhang, J. *et al.* Whole-genome sequencing identifies genetic alterations in pediatric low-grade gliomas. *Nat. Genet.* **45**, 602–612 (2013).
13. Singh, D. *et al.* Transforming fusions of FGFR and TACC genes in human glioblastoma. *Science* **337**, 1231–1235 (2012).
14. Stephens, P.J. *et al.* Massive genomic rearrangement acquired in a single catastrophic event during cancer development. *Cell* **144**, 27–40 (2011).
15. Shlien, A. *et al.* Combined hereditary and somatic mutations of replication error repair genes result in rapid onset of ultra-hypermutated cancers. *Nat. Genet.* **47**, 257–262 (2015).
16. Greco, A. *et al.* The DNA rearrangement that generates the TRK-T3 oncogene involves a novel gene on chromosome 3 whose product has a potential coiled-coil domain. *Mol. Cell. Biol.* **15**, 6118–6127 (1995).
17. Hernández, L. *et al.* TRK-fused gene (TFG) is a new partner of ALK in anaplastic large cell lymphoma producing two structurally different TFG-ALK translocations. *Blood* **94**, 3265–3268 (1999).
18. Bao, Z.S. *et al.* RNA-seq of 272 gliomas revealed a novel, recurrent PTPRZ1-MET fusion transcript in secondary glioblastomas. *Genome Res.* **24**, 1765–1773 (2014).
19. Navis, A.C. *et al.* Identification of a novel MET mutation in high-grade glioma resulting in an auto-active intracellular protein. *Acta Neuropathol.* **130**, 131–144 (2015).
20. Laser-Azogui, A., Diamant-Levi, T., Israeli, S., Roytman, Y. & Tsarfaty, I. Met-induced membrane blebbing leads to amoeboid cell motility and invasion. *Oncogene* **33**, 1788–1798 (2014).
21. Shin, C.H., Grossmann, A.H., Holmen, S.L. & Robinson, J.P. The BRAF kinase domain promotes the development of gliomas in vivo. *Genes Cancer* **6**, 9–18 (2015).
22. Worst, B.C. *et al.* Next-generation personalised medicine for high-risk pediatric cancer patients—The INFORM pilot study. *Eur. J. Cancer* **65**, 91–101 (2016).
23. Chi, A.S. *et al.* Rapid radiographic and clinical improvement after treatment of a MET-amplified recurrent glioblastoma with a mesenchymal-epithelial transition inhibitor. *J. Clin. Oncol.* **30**, e30–e33 (2012).
24. Birchmeier, C., Birchmeier, W., Gherardi, E. & Vande Woude, G.F. Met, metastasis, motility and more. *Nat. Rev. Mol. Cell Biol.* **4**, 915–925 (2003).
25. Gherardi, E., Birchmeier, W., Birchmeier, C. & Vande Woude, G. Targeting MET in cancer: rationale and progress. *Nat. Rev. Cancer* **12**, 89–103 (2012).
26. Brennan, C.W. *et al.* The somatic genomic landscape of glioblastoma. *Cell* **155**, 462–477 (2013).

27. Mak, H.H. *et al.* Oncogenic activation of the Met receptor tyrosine kinase fusion protein, Tpr-Met, involves exclusion from the endocytic degradative pathway. *Oncogene* **26**, 7213–7221 (2007).
28. Cooper, C.S. *et al.* Molecular cloning of a new transforming gene from a chemically transformed human cell line. *Nature* **311**, 29–33 (1984).
29. Yoshihara, K. *et al.* The landscape and therapeutic relevance of cancer-associated transcript fusions. *Oncogene* **34**, 4845–4854 (2015).
30. Diamond, J.R. *et al.* Initial clinical sensitivity and acquired resistance to MET inhibition in MET-mutated papillary renal cell carcinoma. *J. Clin. Oncol.* **31**, e254–e258 (2013).
31. Lai, A.Z. *et al.* Dynamic reprogramming of signaling upon met inhibition reveals a mechanism of drug resistance in gastric cancer. *Sci. Signal.* **7**, ra38 (2014).
32. Truffaux, N. *et al.* Preclinical evaluation of dasatinib alone and in combination with cabozantinib for the treatment of diffuse intrinsic pontine glioma. *Neuro-oncol.* **17**, 953–964 (2015).
33. Mossé, Y.P. *et al.* Safety and activity of crizotinib for pediatric patients with refractory solid tumors or anaplastic large-cell lymphoma: a Children's Oncology Group phase 1 consortium study. *Lancet Oncol.* **14**, 472–480 (2013).

[1]Division of Pediatric Neuro-oncology, German Cancer Research Center (DKFZ), Heidelberg, Germany. [2]Department of Pediatric Oncology, Hematology and Immunology, Heidelberg University Hospital, Heidelberg, Germany. [3]German Cancer Consortium (DKTK), German Cancer Research Center (DKFZ), Heidelberg, Germany. [4]Division of Molecular Genetics, German Cancer Research Center (DKFZ), Heidelberg, Germany. [5]Max Planck Institute for Molecular Genetics, Berlin, Germany. [6]Division of Applied Bioinformatics, German Cancer Research Center (DKFZ), Heidelberg, Germany. [7]Department of Neuropathology, NN Burdenko Neurosurgical Institute, Moscow, Russia. [8]Institute of Molecular Medicine and Cell Research (IMMZ), Faculty of Medicine, University of Freiburg, Freiburg, Germany. [9]Centre for Biological Signalling Studies (BIOSS), University of Freiburg, Freiburg, Germany. [10]Divisions of Molecular Pathology and Cancer Therapeutics, Institute of Cancer Research, Sutton, UK. [11]European Molecular Biology Laboratory (EMBL), Genome Biology Unit, Heidelberg, Germany. [12]Division of Theoretical Bioinformatics, German Cancer Research Center (DKFZ), Heidelberg, Germany. [13]National Center for Tumor Diseases (NCT), Heidelberg, Germany. [14]Department of Neuroradiology, Heidelberg University Hospital, Heidelberg, Germany. [15]Division of Translational Oncology, German Cancer Research Center (DKFZ), Heidelberg, Germany. [16]Genomics and Proteomics Core Facility, German Cancer Research Center (DKFZ), Heidelberg, Germany. [17]Department of Neurosurgery, Heidelberg University Hospital, Heidelberg, Germany. [18]Clinical Cooperation Unit Pediatric Oncology, German Cancer Research Center (DKFZ), Heidelberg, Germany. [19]Department of Neuropathology, University of Heidelberg, Heidelberg, Germany. [20]Clinical Cooperation Unit Neuropathology, German Cancer Research Center (DKFZ), Heidelberg, Germany. [21]Unité Mixte de Recherche du Centre National de la Recherche Scientifique (CNRS) 8203, Laboratoire de Vectorologie et Thérapeutiques Anticancéreuses, Villejuif, France. [22]Department of Pediatric and Adolescent Oncology, Institut Gustave Roussy, Université Paris Sud, Villejuif, France. [23]Department of Pediatrics, McGill University and the McGill University Health Center Research Institute, Montreal, Quebec, Canada. [24]Department of Human Genetics, McGill University and the McGill University Health Center Research Institute, Montreal, Quebec, Canada. [25]Department of Pediatric Hematology and Oncology, Rigshospitalet, Copenhagen, Denmark. [26]Department of Pediatric Hematology and Oncology, 2nd Faculty of Medicine, Charles University and University Hospital Motol, Prague, Czech Republic. [27]Department of Cytogenetics and Reproductive Biology, Farhat Hached Hospital, Sousse, Tunisia. [28]Department of Anatomical and Cellular Pathology, Chinese University of Hong Kong, Hong Kong, China. [29]Department of Pathology, New York University School of Medicine, New York, USA. [30]Department of Neurosurgery, New York University School of Medicine, New York, USA. [31]Department of Pediatrics, New York University Langone Medical Center, New York, USA. [32]Department of Pediatric Oncology and Haematology, Princess Margaret Hospital for Children, Perth, Western Australia, Australia. [33]Telethon Kids Institute, University of Western Australia, Perth, Western Australia, Australia. [34]School of Pediatrics and Child Health, University of Western Australia, Perth, Western Australia, Australia. [35]Department of Neuropathology, Heinrich-Heine-University Düsseldorf, Düsseldorf, Germany. [36]Comprehensive Cancer Center Freiburg CCCF, Medical Center – University of Freiburg, Freiburg, Germany. [37]Deutsches Konsortium für Translationale Krebsforschung (DKTK), Standort Freiburg, Germany. [38]Institute for Pharmacy and Molecular Biotechnology (IPMB), University of Heidelberg, Heidelberg, Germany. [39]BioQuant Center, University of Heidelberg, Heidelberg, Germany. [40]These authors contributed equally to this work. [41]These authors jointly directed this work. Correspondence should be addressed to S.M.P. (s.pfister@dkfz.de), D.T.W.J. (david.jones@dkfz.de) or P.L. (peter.lichter@dkfz.de).

ONLINE METHODS

Patient and tumor samples. Informed consent from all patients as well as an ethical vote (Ethics Committee of the Medical Faculty of Heidelberg) was obtained according to the ICGC guidelines. Tumor tissues were subjected to neuropathological review to confirm histology and tumor cell content.

DNA sequencing. Paired-end library preparation was conducted using Illumina v2 protocols. Genomic DNA (~1 µg) was fragmented to an insert size of ~300 bp with a Covaris device, and size selection was performed using agarose gel excision. Deep sequencing was carried out with Illumina HiSeq 2000 instruments.

RNA sequencing. RNA integrity was evaluated by using a Bioanalyzer 2100 instrument (Agilent). Stranded paired-end libraries were prepared from 1 µg RNA using the Ribo-Zero Gold Kit (Epicentre). One library per lane was sequenced on a HiSeq 2000 instrument with 2 × 51 bp reads. Gene fusion events were detected by RNA-seq read mapping to the human NCBI37/hg19 reference assembly using SOAPfuse[34] and TopHat2-Fusion[35]. High-confidence events were retained after filtering of common artifacts and visual inspection of RNA-seq coverages on fused exons. Fusion transcripts were annotated on the basis of the Ensembl gene annotation (v70). For fusion transcript validation, 50 ng of total RNAs were reverse transcribed, and fused transcripts were amplified using the dART 1-Step RT-PCR Kit (EURx #E0803-02) using primers located upstream and downstream of the transcript breakpoints. RT-PCR products were separated and visualized on 2.5% TBE-agarose gel, excised and purified using the Zymoclean Gel DNA Recovery Kit (Zymo Research). Capillary Sanger sequencing of 30 ng RT–PCR product was performed with 15 pmol primer (Eurofins MWG Operon).

Mapping and analysis. According to the ICGC The Cancer Genome Atlas Pan Cancer Whole Genome workflow, reads were mapped to the 1000 genomes phase 2 assembly of the human reference genome GRCh37 (NCBI build 37.1, downloaded from ftp://ftp.1000genomes.ebi.ac.uk/vol1/ftp/technical/reference/phase2_reference_assembly_sequence) using BWA[36] version 0.7.8 mem with option -T 0. The biobambam package[37] was used to sort the output and to mark PCR duplicates during merging of the per-lane BAM files.

High-level copy number gains were identified by read depth plots and custom Perl scripts.

For detection of single nucleotide variants (SNVs), we used our in-house SNV detection pipeline based on SAMtools mpileup and bcftools[36] version 0.1.19 with parameter adjustments to allow calling of somatic variants with low allele frequency as described previously[38] and heuristic filtering, also as described previously[11].

Short insertions and deletions (indels) were identified with Platypus version 0.7.4 (ref. 39) by providing the tumor and control BAM files. To be of high confidence, somatic calls (control genotype 0/0) are required to have the Platypus filter flag PASS or pass custom filters allowing for low variant frequency using a similar scoring scheme as for SNVs. In detail, we discard candidates with the badReads flag, with alleleBias or strandBias if the variant allele frequency is less than 10%, and indels that have more than two of the remaining flags. In addition, combinations of Platypus non-PASS filter flags, bad quality values, low genotype quality, very low variant counts in the tumor and presence of variant reads in the control were not tolerated.

All mutations are annotated with ANNOVAR[40] version November 2014, with the Gencode version 19 gene model. Additional information is included by overlapping the genomic positions with dbSNP version 141, 1,000 genomes phase 1 integrated calls 20101123 and COSMIC version 66. Only somatic, high confidence SNVs and indels were considered for further analysis. We then extracted nonsilent coding SNVs, SNVs at splice sites and indels that fall into a coding gene or splice site. For defining potential somatic SNVs in the cell lines, we discard SNVs and indels known from 1,000 genomes or with the dbSNP 141 COMMON = 1 flag.

RNA-seq reads were mapped with STAR version 2.3.0e[41] using an index of the 1,000 genomes reference sequence with Gencode version 17 transcript annotations. The output was converted to sorted BAM with SAMtools and duplicates were marked with Picard version tools (http://broadinstitute.github.io/picard/, version 1.90).

Expression levels were determined per gene and sample as reads per kilobase of exon model per million reads (RPKM). As the gene model, RefSeq was used. For each gene, overlapping annotated exons from all transcript variants were merged into nonredundant exon units with a custom Perl script. Nonduplicate reads with mapping quality above zero were counted for all exon units with coverageBed from the BEDtools package[42]. The read counts were summarized per gene, and then divided by the combined length of its exon units (in kilobases) and the total number of reads (in millions) counted in total by coverageBed.

SNVs and indels were annotated with RNA information by generating a pileup of the DNA variant position in the RNA BAM file with SAMtools. The respective genes, as well as genes in high-level copy number gains, were assigned their expression values.

Chromothripsis was scored in accordance with the criteria outlined previously[43].

DNA methylation profiling. For genome-wide assessment of DNA methylation, ICGC_GBM samples (n = 51) were analyzed using the Illumina HumanMethylation450 BeadChip according to the manufacturer's instructions at the DKFZ Genomics and Proteomics Core Facility. In addition, 450k DNA methylation data of 64 reference pediatric glioblastomas described previously[6], 16 normal brain samples as well as seven PXAs was included. DNA methylation probes were filtered as previously described[6]. For unsupervised hierarchical clustering, we selected the 2,052 most variably methylated probes across the data set (s.d. > 0.3). Samples were clustered using 1-Pearson correlation coefficient as the distance measure and average linkage (x-axis). Methylation probes were reordered by hierarchical clustering using Euclidean distance and average linkage (y axis).

Gene expression profiling and classification. Differentially expressed genes (t test: $P < 0.01$) were identified by comparing TFG-MET-overexpressing and empty vector transduced normal human astrocytes (NHAs). Classification of tumor samples studied on the Affymetrix U133 Plus2.0 expression array was performed as described previously[6] using the 840 gene Cancer Genome Atlas signature[44].

***In vitro* studies of MET-fusion-expressing HEK293T and SJ-G2 cells.** HEK293T and human SJ-G2 glioblastoma cells (authors' long-term stocks) were cultured in high glucose Dulbecco's Modified Eagle's Medium (DMEM) (Life Technologies) supplemented with 10% FCS (GIBCO) and penicillin/streptomycin (GIBCO) at 37 °C and 5% CO_2. Cells were trypsinized upon reaching a confluency of 80%. Foretinib (Selleck Chemicals) and temozolomide (University Hospital Pharmacy Heidelberg) was dissolved in DMSO and stored at −20 °C. 3 h before cell harvest, cell culture medium, including inhibitors, was replaced. Cell lines were checked for genotype and for mycoplasma before initiation of experiments.

Coding sequences of wild-type MET, PTPRZ1-MET or TFG-MET were cloned from tumor cDNA into the pcDNA3.1 vector (Life Technologies) introducing a HA tag. HEK293T cells were transfected using TransIT-LT1 transfection reagent (Mirus).

To determine the IC_{50} of foretinib and temozolomide, pediatric glioblastoma cell lines were seeded in a 96-well format (opaque-walled) and incubated for 24 h in DMEM supplemented with 10% FCS (GIBCO) and penicillin/streptomycin (GIBCO) at 37 °C and 5% CO_2. Subsequently, cells were treated with the indicated concentration of foretinib and temozolomide for an additional 24 h before replacing the drug-containing medium and incubated for another 24 h at 37 °C and 5% CO_2. Cell viability was determined in triplicates by using the CellTiter-Glo luminescence cell-viability assay (Promega) according to the manufacturer's instructions using a Mithras LB 940 Microplate Reader. Quantification of anchorage-independent growth of SG-G2 cells was determined by using the CytoSelect 96-well cell transformation assay (Cell Biolabs) according to the manufacturer's instructions after the indicated time period. Foretinib- or DMSO-containing DMEM medium was replaced every 24 h.

Transduction of NHAs. The bicistronic retroviral vector pMIBerry has been described previously[45]. To generate a pMIBerry vector encoding C-terminally HA-tagged TFG-MET, this cDNA was amplified from pLVX/TFG–MET-puro

doi:10.1038/nm.4204

using Phusion polymerase (Finnzymes) and the oligonucleotides XhoITFG–METfwd 5′- AATTCTCGAGATGAACGGACAGTTGGATCTAAGTGGGAAGCTAATC-3′ and BamHITFG–METrev 5′-TTAAAGGATCCTCTAGACTAGGCATAGTCAGGCACGTCATAAGGATATG-3′ using the standard protocol supplied by the manufacturer. PCR amplicons were gel purified, digested with XhoI and BamHI and subcloned into XhoI/BamHI linearized pMIBerry. Sanger sequencing confirmed the TFG-MET cDNA sequence.

The culture and transfection of Plat-E cells, as well as the generation of retroviral supernatants, have been described previously[45]. The immortalized astrocytes were derived from primary normal human astrocytes (NHA; lot lumber 5F1118; Lonza) and were grown in designated astrocyte medium (Lonza) as directed by the manufacturer. For immortalization, 2×10^6 NHA cells were transiently transfected with 2 µg of pQCXIN/ecoR and the 'primary neurons' nucleofector kit (Lonza). This procedure allows for transient expression of the ecotropic receptor used by murine retroviruses, which in turn allows for the infection with ecotropic viral particles as described previously[46]. 2 d later, nucleofected cells were infected with the Simian Virus 40 large T antigen (TAg) expression vector pQCXIN/TAg[45]. Tag-expressing NHAs were positively selected by TAg-mediated suppression of naturally occurring senescence. Subsequently, 2×10^6 cells were transfected with 2 µg of the plasmid pQCXIN/ecoR. Nucleofected NHA/TAgs were selected with 2 mg/ml G418. The resulting NHATAg-ecoR cells were then incubated with a 1:1 dilution of retroviral supernatants from the indicated pMIG or pMIBerry Plat-E transfectants with astrocyte medium. Infected cells were identified by their dsRed2 autofluorescence 48 h postinfection and monitored by flow cytometry.

Immunofluorescence. Infected NHA/TAg-ecoR cells were plated on chamber slides (Becton Dickinson) and grown until reaching subconfluency (~72 h). Cells were then fixed with 4% paraformaldehyde solution for 15 min at 20–22 °C. Subsequently, F-actin staining (Phalloidin Alexa 488 (Cell Signaling)) and DAPI ProLong Gold (LifeTechnologies) were applied according to manufacturers' protocols. Stained cells were imaged with the ZEISS Axio-observer Z1 bright field microscope plus ApoTome 2 with a connected AxioCamMRm. Images were taken with a 40× PlanNeoFluar 1.3 oil objective using the AxioVision Rel 4.8 software.

Western blotting. Protein extract of cell pellets were generated by using RIPA buffer (Sigma-Aldrich) including the Halt Phosphatase Inhibitor Cocktail (Thermo Scientific). Electrophoretic separation of protein samples was performed using 4–12% gradient NuPAGE Bis-Tris Precast Gels (Life Technologies) followed by protein transfer to a polyvinylidene fluoride (PVDF) membrane using a full wet-blotting procedure. Antibodies against the following antigens were applied: HA-tag (3724; Cell Signaling; 1:1,000), MET (8198; Cell Signaling; 1:1,000), pMET (3077; Cell Signaling; 1:1,000), pERK1/2 (4370; Cell Signaling; 1:2,000) RAB11 (5589; Cell Signaling; 1:2,000) and GAPDH (CB1001; Calbiochem; 1:10,000). Validation of all antibodies is provided on the manufacturer's website.

Fluorescence *in situ* hybridization (FISH). Dual-color interphase fluorescence *in situ* hybridization was performed on FFPE-embedded tissue sections using a PTPRZ1 (RP11-207K20; green) and MET (RP11-95I20; red) specific probe. For each tumor, 200 interphase nuclei were analyzed microscopically.

Animal studies. All animal experiments were conducted in accordance with legal regulations and approved by the regional council (Regierungspräsidium Tübingen; G-4/11, G-238/12, G-163/14). Mice were housed in IVC caging in the Center for Preclinical Research of the DKFZ and monitored daily for the presence of tumor-related symptoms. Sample sizes were chosen to minimize the number of animals required to get significant results.

RCAS-based tumor model. For tumor induction using RCAS-based somatic gene transfer, the HA-tagged TFG-MET fusion was PCR amplified and cloned into the RCASBP(A) backbone using ClaI and NotI restriction sites. Virus production was done in DF-1 chicken fibroblasts by transfection using FuGene HD (Promega) according to the manufacturer's protocol. Ntv-a, Ntv-a; *Cdkn2a*$^{-/-}$; *Pten*$^{fl/fl}$, Ntv-a; *Trp53*$^{-/-}$ or or Ntv-a; *Trp53*$^{-/-}$ pups were injected at postnatal day 0 with 100,000 virus-producing cells into the left cerebral hemisphere using a Hamilton syringe.

Xenograft and preclinical studies. Cells derived from Ntv-a; *Cdkn2a*$^{-/-}$; *Pten*$^{fl/fl}$ animals injected with RCAS-TFG-MET virus or SJ-G2 tumor cells were labeled with luciferase using pGF lentivirus and subsequently GFP-positive cells were FACS sorted. 500,000 SJ-G2 cells or 100,000 TFG-MET-RCAS cells were transplanted into the striatum of 6–8-week-old female C.B-17 SCID (coordinates 2.5 mm lat., 1 mm caud., 3 mm ventr. relative to bregma; animals obtained from Charles River or Janvier Labs, respectively). Animals received pre-emptive Carprofen analgesia and were anesthetized with Isoflurane. Postsurgically, analgesia was continued with Carprofen. For luciferase imaging, animals were injected with 100 µl Luciferin solution (15 mg/ml, Promega) and imaged using an IVIS100 or IVIS Lumina luminescence imager with an exposure time of 5 min. For the treatment studies, Foretinib was dissolved in DMSO and then diluted in 5 mg/ml hydroxypropyl methylcellulose/0.05% SDS. Animals were randomized to treatment or control strata according to their luminescence signals. 60 mg/kg Foretinib or vehicle was administered nonblinded by oral gavage every other day starting at day 7 after surgery. Kaplan–Meier analysis was done using GraphPad Prism, and statistical significance was calculated using a log–rank test.

MRI. MRI was undertaken on a 9.4T horizontal bore NMR scanner (BioSpec 94/20 USR, Bruker BioSpin GmbH, Ettlingen, Germany) with the CryoProbe head coil. A 15 slice T1-weighted RARE (rapid acquisition with relaxation enhancement) sequence, after an intraperitoneal injection of 100 µl of a 1:10 dilution of Omniscan (0.5 mmol/ml, GE Healthcare Buchler GmbH), was acquired. The MRI parameters were as follows: TR/TE = 1,000/6 ms, matrix = 200 × 150, resolution = 0.1 × 0.1 mm, slice thickness/gap = 0.3/0.3 mm, NA = 2; RARE factor = 1; total acquisition time = 5 min.

34. Jia, W. *et al.* SOAPfuse: an algorithm for identifying fusion transcripts from paired-end RNA-Seq data. *Genome Biol.* **14**, R12 (2013).
35. Kim, D. *et al.* TopHat2: accurate alignment of transcriptomes in the presence of insertions, deletions and gene fusions. *Genome Biol.* **14**, R36 (2013).
36. Li, H. & Durbin, R. Fast and accurate short read alignment with Burrows-Wheeler transform. *Bioinformatics* **25**, 1754–1760 (2009).
37. Tischler, G. & Leonard, S. biobambam: tools for read pair collation based algorithms on BAM files. *Source Code Biol. Med.* **9**, 13 (2014).
38. Jones, D.T. *et al.* Dissecting the genomic complexity underlying medulloblastoma. *Nature* **488**, 100–105 (2012).
39. Rimmer, A. *et al.* Integrating mapping-, assembly- and haplotype-based approaches for calling variants in clinical sequencing applications. *Nat. Genet.* **46**, 912–918 (2014).
40. Wang, K., Li, M. & Hakonarson, H. ANNOVAR: functional annotation of genetic variants from high-throughput sequencing data. *Nucleic Acids Res.* **38**, e164 (2010).
41. Dobin, A. *et al.* STAR: ultrafast universal RNA-seq aligner. *Bioinformatics* **29**, 15–21 (2013).
42. Quinlan, A.R. & Hall, I.M. BEDTools: a flexible suite of utilities for comparing genomic features. *Bioinformatics* **26**, 841–842 (2010).
43. Korbel, J.O. & Campbell, P.J. Criteria for inference of chromothripsis in cancer genomes. *Cell* **152**, 1226–1236 (2013).
44. Verhaak, R.G. *et al.* Integrated genomic analysis identifies clinically relevant subtypes of glioblastoma characterized by abnormalities in PDGFRA, IDH1, EGFR and NF1. *Cancer Cell* **17**, 98–110 (2010).
45. Röring, M. *et al.* Distinct requirement for an intact dimer interface in wild-type, V600E and kinase-dead B-Raf signalling. *EMBO J.* **31**, 2629–2647 (2012).
46. Eisenhardt, A.E. *et al.* Functional characterization of a BRAF insertion mutant associated with pilocytic astrocytoma. *Int. J. Cancer* **129**, 2297–2303 (2011).